Applied Catalysis B: Environmental 272 (2020) 118969

Contents lists available at ScienceDirect

Applied Catalysis B: Environmental

journal homepage: www.elsevier.com/locate/apcatb

Photocatalytic degradation mechanism of gaseous styrene over Au/TiO_2@CNTs: Relevance of superficial state with deactivation mechanism

Weiping Zhang, Guiying Li, Hongli Liu, Jiangyao Chen, Shengtao Ma, Meicheng Wen, Jiejing Kong, Taicheng An*

Guangdong Key Laboratory of Environmental Catalysis and Health Risk Control, Guangzhou Key Laboratory of Environmental Catalysis and Pollution Control, School of Environmental Science and Engineering, Institute of Environmental Health and Pollution Control, Guangdong University of Technology, Guangzhou, 510006, China

ARTICLE INFO

Keywords:
Photocatalytic
VOCs elimination
Coke formation
Intermediates accumulation
Deactivation mechanism

ABSTRACT

Commonly, the efficient and durable activities of photocatalyst are fundamental requirement for elimination of VOCs in industrial application. However, the photocatalytic activity of materials was gradually decreased due to change of superficial state, such as intermediates growth and coke accumulation. Results showed that intermediate accumulation was predicted to be one of the key factors for photocatalysts deactivation on all type of as-prepared photocatalyst. The further dehydration of accumulated intermediates may cause carbonaceous deposits (coke). The results of superficial state showed that coke could bring great negative effects for Au/TiO_2@CNTs while positive effects for TiO_2 on formation of oxidation radicals. However, the fresh VOCs could suffer competitive oxidation reaction with their intermediates and coke, which would subsequently exacerbate accumulation of coke and intermediates, and then jointly worsen the photocatalytic activity and finally caused the deactivation. This work provided a new insight into revealing the deactivation mechanism of photocatalyst during VOCs purification.

1. Introduction

Volatile organic compounds (VOCs), such as styrene, extensively released from industrial manufacture, disassemble e-waste, volatilization of coating, plastic products and etc. Long-term exposure to low concentration of VOCs has shown to cause series of acute and chronic disease on human [1,2]. Hence, the investigation of VOCs elimination with economic efficiency has become the hot topic in the environmental field [3,4]. Among eco-friendly technologies to destroy hazardous VOCs, the advanced oxidation processes (AOPs) represent an effective alternative to traditional chemical technologies [5–7]. In the research field of photocatalytic oxidation with TiO_2 to confer partial or total oxidation of gaseous pollutants to harmless intermediates is one of the most promising environment-benign methods to abate VOCs [8–10]. The formation of free radicals related to separation of e^--h^+ pairs on TiO_2 can impact on the mineralization of VOCs to H_2O and CO_2 [11,12]. However, TiO_2 shows low solar harvest and high recombination of photo-generated e^--h pairs, resulting in decreasing photocatalytic activity to VOCs [13].

Among of the TiO_2-based photocatalyst system with visible-light response, Au/TiO_2 showed a high absorption of the visible light because of the surface resonance plasmon (SPR), which exhibited high efficiency photocatalytic reaction of VOCs degradation [14–16]. However, non-volatility intermediates may be generated from the incomplete oxidation of VOCs accumulated on the surface of photocatalysts on Au/TiO_2 due to its lower specific surface area and slower mass transfer [17]. These intermediates would be transferred into carbonaceous deposits (coke, involving long-chain organics) due to the absence of free radicals during the further deep oxidation process, resulting in the decrease of photocatalytic activity or deactivation of photocatalysts [18–20].

Recently, carbon nanotube-semiconductor composites were found having the unique superiority in synergetic photocatalytic degradation of organic contaminant because of their excellent properties of electrical properties, high adsorption capacity, and chemical and thermal stability [21–25]. Therefore, it is urgently desired to combine CNTs with Au/TiO_2 NPs for fabricating Au/TiO_2@CNTs composite to decrease the deactivation procedure of photocatalyst [26–28]. The decreased photocatalytic activity is a complex and continuous reaction processes, and the changes of superficial structure and properties of photocatalysts are found to be the key factor for the photocatalytic performance [29,30]. Hence, it is very essential to deeply investigate

* Corresponding author.
E-mail address: antc99@gdut.edu.cn (T. An).

https://doi.org/10.1016/j.apcatb.2020.118969
Received 18 February 2020; Received in revised form 1 April 2020; Accepted 3 April 2020
Available online 10 April 2020

the changes of superficial properties, and associated reasons as well as dominant factor on the deactivation of the photocatalyst. Especially, how the coke formation associated with accumulation of intermediates happened and affected the transfer and separation of interfacial charges, LSPR of Au NPs, generation of free radicals, oxygen vacancies and etc.

In this work, styrene was used as typical VOCs, and Au/TiO_2@CNTs composite materials was employed as photocatalyst, then the influence of superficial state, such as coke formation and accumulation of intermediates, on the structure and properties of this composite photocatalysts was systematically investigated. Numerous analytical techniques were employed to investigate the thermal stability, surface structure, optical properties, oxygen vacancies, separation of photogenerated e^--h^+ pairs, photoelectrochemical properties, and generation of free radicals and activation of the chemisorbed oxygen to reveal the influence and weight the function of coke. In addition, the type and species of accumulated intermediates on different photocatalysts were also identified to reveal their internal relationship between the superficial state and the composition of photocatalysts as well as the photocatalytic degradation mechanism illumination. Finally, this work gave systematic explanations on the deactivation performance and provided a new insight into revealing the deactivation mechanism of used photocatalyst.

2. Experimental section

2.1. Synthesis and characterization of photocatalysts

Approximately 0.5 g of CNTs (95 %, 8–15 nm, Beijing Boyu-Gaoke New Material Co., Ltd) were functionalized with a mixture of nitric acid (65 %－68 %, Guangzhou chemical reagent factory) and concentrated sulfuric acid (95 %－98 %, Guangzhou chemical reagent factory) with a volume ratio of 1:3 under the room temperature for 5 h. The above mixed dispersion was treated at 70 °C for 1 h and then 90 °C for 0.5 h. The obtained mixture was filtered and washed by mixed solution of water and EtOH (Volume ratio = 1:3). The final functional CNTs were treated by freeze-drying for 12 h and thermal treatment at 60 °C for 10 h. The Au/TiO_2@CNTs composites were prepared using a micro/nano–bubble assisted method as recommended in our early reference [17] and the detailed procedure was described in the Supporting Information (SI).

The morphologies of the as–synthesized samples were observed using transmission electron microscope (TEM, Hitachi, Japan) and scanning electron microscopy (SEM, ZEISS Merlin, German). The phases of the samples were characterized using D/MAX-Ultima IV X–ray diffractometer (XRD, Rigaku, Japan) with a Cu tube for generating Cu Kα radiation (λ = 1.5418 Å). The surface electronic states of the samples were assessed with an Escalan 250Xi X-ray Photoelectron spectroscopy (XPS, Thermo Fisher, America). The functional groups of the samples were analyzed by a Nicolet6700 Fourier transform–infrared spectrometer (FT–IR, Nicolet, America). Molecular structure and chemical compositions of the as–synthesized samples were analyzed by a UV Laser Raman Spectroscopy (Raman, HORIBA Jobin Yvon, France). Electron paramagnetic resonance (EPR) experiments were performed to measure the radical species using a Bruker EMXPlus spectrometer operating at an X-band (9.8 GHz), equipped with a cylindrical cavity operating at 100 kHz field modulation. The presence and mobility of oxygen species on the samples were analyzed with temperature–-programmed desorption of oxygen (O_2-TPD) and carried out on a Multifunctional adsorption instrument (TP-5078, Tianjin Xianquan, China). Thermal stabilities of photocatalysts were performed on a TGA-2 thermal gravimetric analyzer (TGA, METTLER TOLEDO, Switzerland). UV–vis diffuse reflectance spectra (DRS) were collected on an Agilent Cary 300 spectro–photometer with $BaSO_4$ as the standard of reflectance. The fluorescence spectra were collected with an FS5 fluorescence spectrophotometer (Edinburgh, England) with an excitation wavelength of 321 nm at wavelengths ranging from 330 to 600 nm. Time-resolved PL tests were measured using a time-correlated single photon counting (TCSPC) system. Samples were photoexcited by a 380 nm laser beam (EPLED-380), and the detection wavelength was 465 nm. The EPR signal of the radical species was measured by a Bruker EMXPlus spectrometer under room temperature. The photoelectrochemical properties were measured by a CHI650 electrochemical analysis instrument equipped with a three-electrode electrochemical setup, and the details are provided in SI.

2.2. Photocatalytic degradation of gaseous styrene

Photocatalytic activity of as-prepared samples was performed in a photocatalytic reaction system (Zhongjiao-jinyuan Science and Technology Co. Ltd., China) equipped with a gas distributing system provided the gaseous styrene (28 ± 2 ppmv) operating in a continuous flow through mode. During photocatalytic process, 0.1 g of as-synthesized powders was filled in a custom-made cubic quartz glass reactor (1.5 cm × 1.0 cm × 0.1 cm), top of which was a xenon lamp (300 W) fixed vertically with distance of 9 cm. Before irradiation, adsorption equilibrium of gaseous styrene on photocatalyst was achieved. Gas was sampled at given intervals with an auto-feeding device, and gas sample (1 mL) was injected into a gas chromatography (Shanghai Kechuang Chromatographic instrument Co. Ltd, China) with a capillary column (30 m ×0.32 mm ×0.5 μm) for concentration determination. Simultaneously, the yield of carbon dioxide was detected by a GC900 gas chromatography (Shanghai Kechuang Chromatographic instrument Co. Ltd, China). The generated intermediates were analyzed by GC–MSD equipment, and the details are also shown in SI.

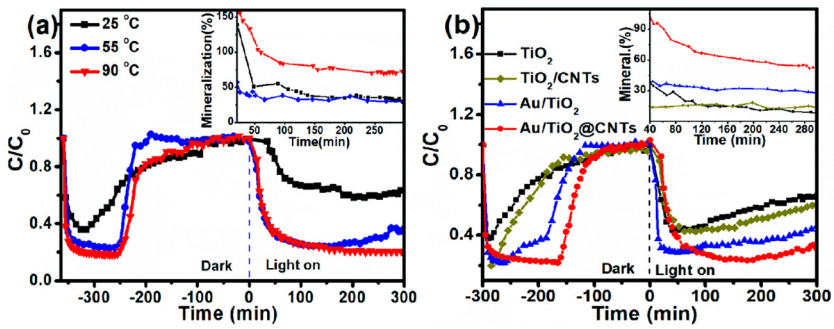

Fig. 1. Photocatalytic performance of Au/TiO_2@CNTs composites with different synthesized temperature (a) and comparison plots of TiO_2, TiO_2/CNTs, Au/TiO_2, and Au/TiO_2@CNTs (b).

3. Results and discussion

3.1. Enhanced photocatalytic performance of TiO_2 by synergetic effect of Au NPs and CNTs

The photocatalytic activity of Au/TiO_2@CNTs was evaluated by gaseous styrene degradation with a continuous flow mode. Fig. 1a shows the photocatalytic degradation and mineralization curves of Au/TiO_2@CNTs composites with different synthesized temperature. It can be clearly seen that the degradation efficiency as well as the mineralization efficiency were gradually enhanced with increasing the synthesized temperature, and the high-level photocatalytic activity with persistent stability was obtained when the synthesized temperature was 90 °C. This is mainly because intimate structure corresponding to interfacial electron transfer might be formed under high temperature, which has been confirmed by our previous report [17]. As compared, photocatalytic performances of other photocatalysts such as TiO_2, TiO_2/CNTs and Au/TiO_2 were also displayed in Fig. 1b [17]. The enhanced photocatalytic activity of Au/TiO_2@CNTs is observed as compared with TiO_2, TiO_2/CNTs and Au/TiO_2. This can be attributed to the synergetic effects of nano Au/TiO_2 and CNTs after TiO_2 decorated with Au NPs and CNTs. To verify this view, more evidences are provided as follow. The element valence of Ti 2p, O 1s, C 1s, and Au 4f are identified from the deconvolution plots of XPS (Fig. S1), which firstly confirm the formation of ternary Au/TiO_2@CNTs composite [27,31–33]. Our previous report also affirmed the chemical bonds formed between Au/TiO_2 and CNTs, which was certainly beneficial for the charge transfer [17]. Besides, the interfacial structure features from SEM and TEM results (Fig. 2a and c) indicate that the uniform network structures are formed due to the formation of ternary Au/TiO_2@CNTs composite photocatalyst, which will promote the mass-transfer of gaseous pollutants as-compared with block TiO_2 (Fig. 2b). The contact structure between Au/TiO_2 NPs and CNTs can be also confirmed from the HR-TEM of Au/TiO_2@CNTs (Figs. 2d and S2). Meanwhile, both the TiO_2 and Au NPs are highly crystallized, and lattice spacing of 0.248 and 0.365 nm are assigned to Au (111) and TiO_2 (101) crystalline lattices, respectively. These results were also confirmed by XRD results of Au/TiO_2@CNTs (Fig. S3) [28,34,35]. That's to say, the contact structure with high crystallization would be very conducive for the photogenerated e^- transferred from Au or TiO_2 to CNTs, and improve photocatalytic activities [26,36]. Further, the enhanced visible-light adsorption and separation of photo-generated charges were observed from the UV–vis DRS and fluorescence spectrum (Figs. S4 and S5). Noted that, Au/TiO_2@CNTs and Au/TiO_2 show a strong absorption within 500–750 nm visible region as compared with pristine TiO_2 [37,38]. PL spectra results showed that PL intensity greatly decreased after TiO_2 decorated with CNTs and Au NPs, which indicates the synergetic effect of CNTs and Au NPs on improving the separation and transfer of photogenerated e^--h^+ pairs on TiO_2 as well as the results of photoelectrochemical properties demonstrated (Fig. S6) [39]. In addition, time-resolved PL spectra were also evaluated with a TCSPC system (Fig. S7). As displayed in Table S1, the shorter lifetimes of Au/TiO_2, TiO_2/CNTs and Au/TiO_2@CNTs as compared with pristine TiO_2 indicates the better charge transfer and separation on Au/TiO_2, TiO_2/CNTs and Au/TiO_2@CNTs, which confirm the excellent electron mobility of Au NPs and CNTs [40,41]. Meanwhile, the Au/TiO_2@CNTs has a shortest lifespan (0.911 ns) than other photocatalysts, indicating the efficient charge transfer and separation on Au/TiO_2@CNTs composite [17,40,42]. These all results provided the evidence on the efficient light adsorption, photogenerated charges transfer and separation, indicating the synergetic effects of Au NPs and CNTs on enhancing photocatalytic activities of TiO_2.

3.2. Intermediates identification and photocatalytic degradation mechanism

It was noted that the photocatalytic degradation and mineralization efficiencies steadily decreased with prolonging radiation time, especially on TiO_2, Au/TiO_2 and TiO_2/CNTs. The decreased photocatalytic performance might be attributed to the changes of superficial state such as accumulation of intermediates [18,43]. Hence, to better understand the reason for the decrease of photocatalytic activities, it is necessary to explore the relevance of photocatalytic activities and the accumulation

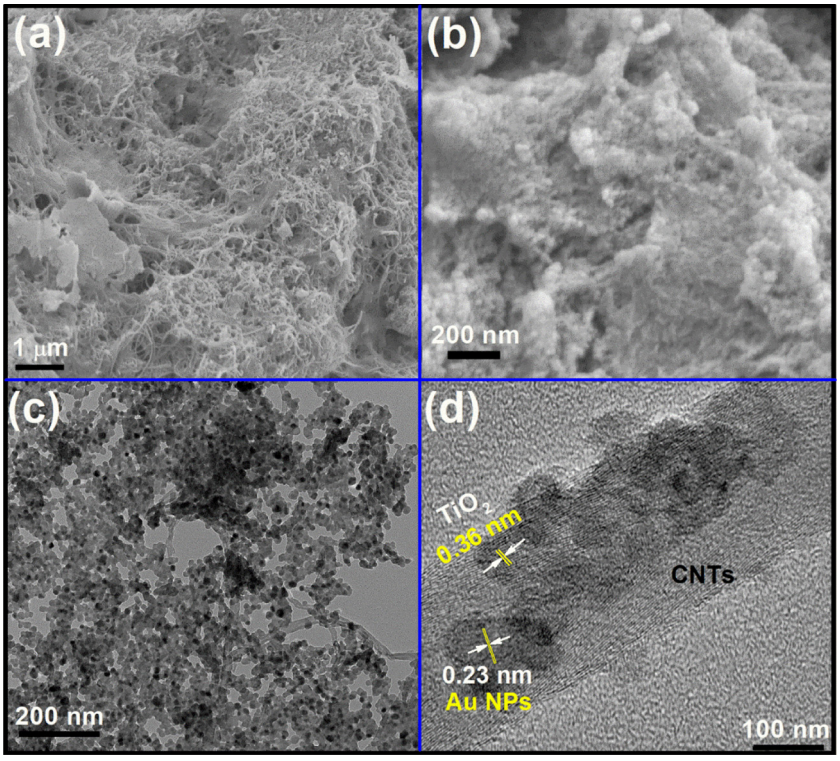

Fig. 2. Morphologies of as-prepared samples: SEM image of Au/TiO_2@CNTs (a) and TiO_2 (b), TEM (c), and HRTEM images (d) of Au/TiO_2@CNTs.

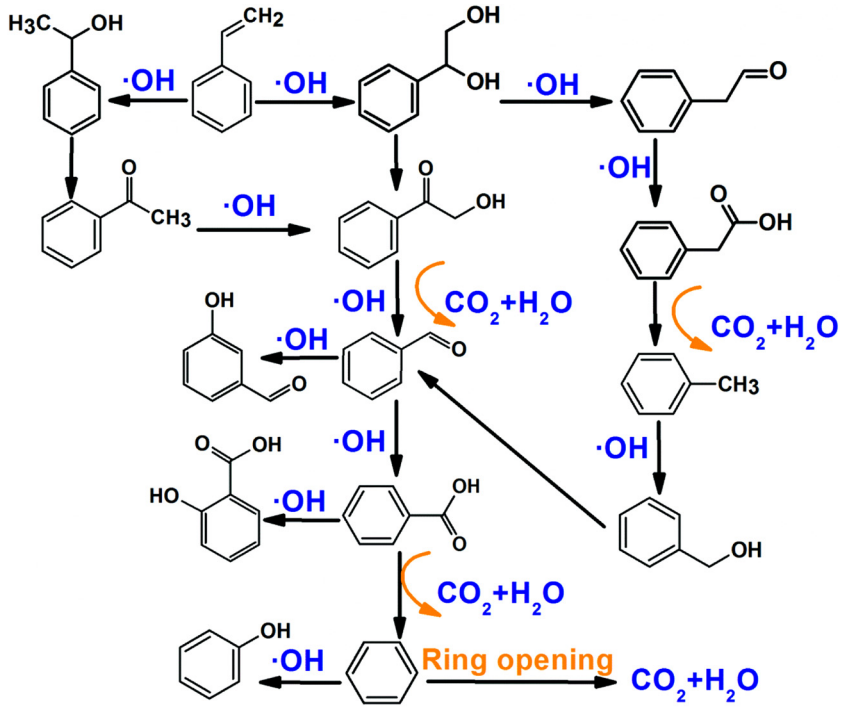

Fig. 3. Possible photocatalytic degradation mechanism of gaseous styrene degradation on Au/TiO_2@CNTs composites.

of intermediates. Here, the identifications and accumulation amounts of intermediates were investigated using a quantitative reaction system with same concentration and volume of gaseous styrene. As shown in Fig. S8a and b, the Au/TiO_2@CNTs show highest photocatalytic degradation and mineralization efficiencies with the degradation order of Au/TiO_2@CNTs > Au/TiO_2 > TiO_2/CNTs > TiO_2 and the mineralization order of Au/TiO_2@CNTs > TiO_2/CNTs > Au/TiO_2 > TiO_2, suggesting the synergistic contribution of Au NPs and CNTs to the photocatalytic performance. Meanwhile, the main degradation intermediates produced on used photocatalysts were identified using GC-MSD method, and displayed in Tables S2, S3 and Fig. S9 (all of the main intermediates are double-confirmed by the standard samples. It is noted that many numerous intermediates, such as aromatic alcohol, aromatic ketone, aromatic acid and aromatic aldehyde, with high molecular weight, complex structure and high boiling point are absorbed onto photocatalysts. Based on this, the photocatalytic reaction mechanism is predicted in Fig. 3. As previous reported, the degradation of styrene is closely related with dehydrogenation reaction of hydroxyl radicals ($^{\cdot}$OH) [44]. This because the initial reactive site of styrene molecule could be activated through the attack of $^{\cdot}$OH due to its high activation energy, and then activated styrene would be mineralized to be CO_2 and H_2O by the further dehydrogenation, chain scission and ring-opening reaction. Here, the relative concentrations of the intermediates are also calculated and displayed in Fig. S10. It is noted that Au/TiO_2@CNTs has the lowest accumulation of intermediates and highest photocatalytic activities than pure TiO_2 (highest accumulation of intermediates and highest photocatalytic activities) because of its high specific surface area and fast mass transfer, which will accelerate the deep oxidation of intermediates into CO_2 and H_2O. However, these generated intermediates with high boiling point and low volatility will occupy the active reaction sites and depress the deep oxidation process with the photocatalytic reaction continued [18,44]. The reason can be explained as follows: 1) the intermediates could occupy the adsorption sites of photocatalysts, leading to its competitive degradation with gaseous styrene; 2) the incomplete oxidation reaction would increase the accumulation of intermediates and then depress the formation of oxidation radicals [18,19]. Hence, the accumulation of intermediates is predicted to be the most important influenced factors to the decrease in catalytic activity and catalysts deactivation during the photocatalytic degradation of VOCs.

In fact, the reasons why the photocatalysts deactivation are not only depended on the accumulation of intermediates, but also depended on the generation of coke. Some previous reports demonstrated that showed that coke was formed on the surface of photocatalyst during the photocatalytic degradation of VOCs, implying that the photocatalyst deactivation should be ascribed to the accumulation of recalcitrant carbonaceous residues [19,45,46]. The coke is very different with graphitic carbon, and its poor conductivity and numerous defects will bring many adverse effects on the photocatalytic performance of photocatalyst, such as light masking effect, high recombination of photogenerated e^--h^+ pairs, and reduce adsorption as well as mass-transfer of VOCs. To confirm these consumptions, the catalytic performances of used photocatalysts are also measured repeatedly (Figs. S8c and d). It was found that the degradation efficiencies of styrene onto used TiO_2 and Au/TiO_2@CNTs all decreased, which was attributed to competitive degradation of styrene and coke. Due to closer to the active sites, the coke can be firstly degraded but the degradation of styrene is significantly hindered during photocatalytic process. As for the mineralization results displayed, the mineralization efficiency of used Au/TiO_2@CNTs is much higher than that of original Au/TiO_2@CNTs and is even over 100 %. That is, the generation of CO_2 can be from the mineralization of both styrene and coke. Especially, the advanced oxidation of coke may substantially enhance the CO_2 concentration. Moreover, TiO_2 used has very high mineralization efficiency, suggesting that the presence of not so much coke could accelerate the advanced oxidation due to more free radicals taking part in the photocatalytic reactions. In addition, the adsorbed intermediates on the surface of Au/TiO_2@CNTs and TiO_2 at 2 h of degradation time are identified and displayed in Fig. S11 and Table S4. Noted that, the used TiO_2 still shows higher accumulation of intermediates than that of used Au/TiO_2@CNTs, and few adsorbed intermediates are still detected on the surface of used catalyst as compared with original one. Besides, as the adsorbed sites are occupied by the coke, the new-produced intermediates are become more difficultly attached to the surface of

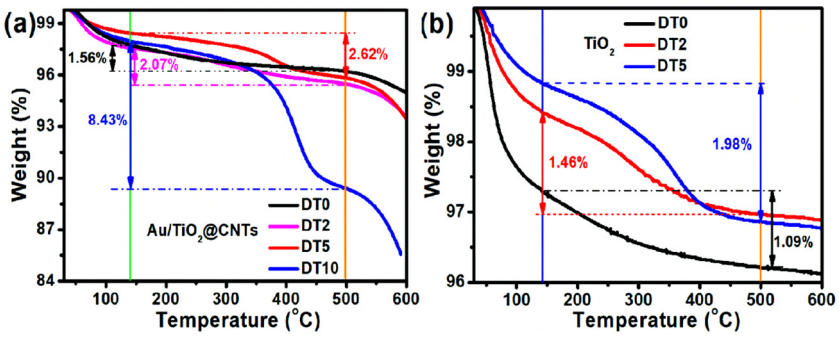

Fig. 4. TGA curves of Au/TiO_2@CNTs (a) and TiO_2 (b). (Mass of each sample: 10 mg).

photocatalysts. This could be one of the important reasons why the decrease of degradation efficiency of styrene besides the accumulated adsorbed intermediates on used catalysts.

3.3. Superficial state change and deactivation mechanism of photocatalysts

In summary, the accumulation of intermediates and then coke formation were predicted to be the key reason for deactivation mechanism of photocatalysts. However, to deeply understand the coke effects on deactivation process, the dependence of the degradation activity on superficial state changes of used photocatalysts was explored by numerous analysis technologies. First of all, the coke formed in the used photocatalysts with different degradation time (DT) was tested by thermogravimetry method. Before the test, the photocatalysts were treated by a series of steps to remove the soluble intermediates based on the GC-MS detection, and the detailed results are described in the SI. As shown in Fig. 4a, the weight loss of used Au/TiO_2@CNTs was calculated as 1.56 % (DT was 0 h, defined as DT0), 2.07 % (DT was 2 h, defined as DT2), 2.62 % (DT was 5 h, defined as DT5), and 8.43 % (DT was 10 h, defined as DT10), which were increased with increasing degradation time. For TiO_2, the weight loss of 1.46 % (DT2) and 1.98 % (DT5) are observed from Fig. 4b. This phenomenon could be also found in Au/TiO_2 (Fig. S12a), TiO_2/CNTs (Fig. S12b), suggesting that the carbonaceous deposits (coke) was formed on the surface of all photocatalysts during photocatalytic process although their different structure and composition. As previous reported, the carbonaceous deposits (coke) with high content of carbon can be speculated that the accumulated intermediates are incompletely oxidized due to their difficult degradation or absence of enough oxidation radicals [14,18,19,47]. The relative contents of coke on used Au/TiO_2@CNTs with different degradation time were also analyzed by XPS semiquantitative method. According to the high-resolution spectra, the atomic percent of C 1s, O 1s, Ti 2p and Au 4f were calculated to be 67.25 %, 22.57 %, 10.13 % and 0.05 % at DT0, and were 69.95 %, 21.96 %, 8.04 % and 0.06 % at DT10, respectively (Table S5). The atomic percent of C 1s in DT10 was higher than that of DT0, which further confirmed the coke formation on Au/TiO_2@CNTs. It is noted that the peak intensity ratio of 285.6 eV/284.6 eV in DT10 is much higher than that of DT0 (Fig. 5a), indicating more defect sites are generated after photocatalytic reaction [27]. Meanwhile, the characteristic peaks of 459.6 eV and 465.4 eV shift to 459.5 eV and 465.2 eV comparably before and after degradation reaction (Fig. 5b), which can be attributed to the C—O species of coke coupling with TiO_2 to form chemical interface.

The change of functional group on Au/TiO_2@CNTs was analyzed by FTIR (Fig. 6). Obviously, new functional groups of C=C and C=O located at 1640, 1467, 1581 and 1404 cm^{-1} are observed as compared with fresh photocatalyst, which is speculated to be the functional groups of coke [48–50]. The high peak intensity of C=C and C=O were observed with increasing the degradation time, confirming that a large amount of coke is generated after long-term photocatalytic reaction as TGA results described. Further, Influence of coke on crystal structure of different compositions also characterized by XRD and showed that TiO_2 and Au were almost not changed after 10 h of photocatalytic reaction, suggesting the stable crystal structure of Au/TiO_2@CNTs (Fig. S13). That is, the coke occurred only on the surface of Au/TiO_2@CNTs, and would not affect its internal crystal structure at short degradation duration. The interaction changes of different compositions on Au/TiO_2@CNTs were further confirmed by Raman spectra. After photocatalytic reaction, the vibrational modes of $B_{1g(1)}$, A_{1g} + $B_{1g(2)}$ and $E_{g(2)}$ shift from 395, 513, and 637 cm^{-1} to 391, 507, and 627 cm^{-1}, respectively, for the used Au/TiO_2@CNTs photocatalyst (Fig. 7a). The slight blue shifts can be attributed to the C=O or C—O species of coke were coupled with TiO_2 during photocatalytic process, leading to vibrational energy of related modes becoming lager, which is consistent with XPS results [51,52]. Typically, two Raman bands with weaker intensity called 2D and D + G located at 2500–3100 cm^{-1} were observed from Fig. 7b. 2D band is ascribed to active crystalline graphitic materials and it is sensitive to the π-band in the graphitic electronic structure, while the combination mode of D + G is induced by disorder [53,54]. Previous literature reported that it can be easy to distinguish the electronic conjugation of crystalline graphitic materials from the intensity ratios of I_{2D}/I_{D+G} [55,56]. The integrated data showed that I_{2D}/I_{D+G} of 7.99 at DT0 was higher than that of 0.86 at DT10, suggesting that more amorphous carbon was generated and deposited onto

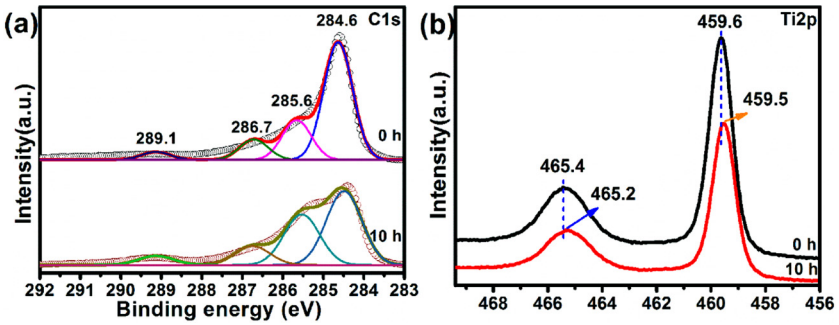

Fig. 5. High-resolution XPS spectra of C 1s (a) and Ti 2p (b) on Au/TiO_2@CNTs composites with different degradation time.

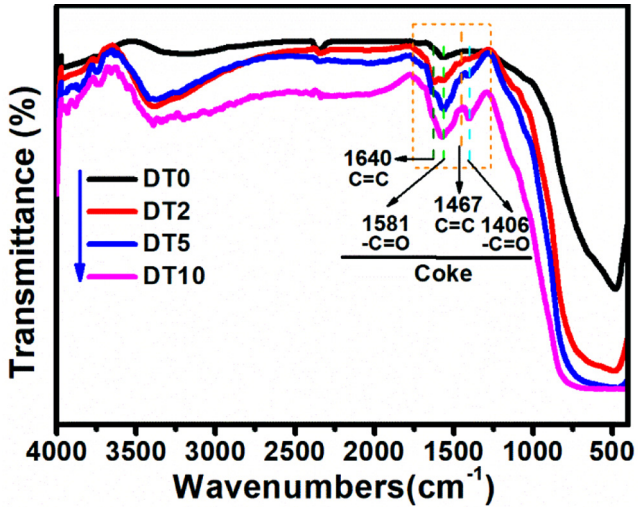

Fig. 6. Changes of functional groups on Au/TiO_2@CNTs composites at different degradation time.

the photocatalyst after degradation reaction.

EPR spectra of Au/TiO_2@CNTs powder used after different degradation duration are measured in Fig. S14 for investigating the oxygen vacancies. All used samples show unambiguously intense EPR signals at around g_{yy} = 2.004, which can be attributed to e^- trapped at TiO_2 oxygen vacancies [57–59]. The signals at g_{zz} = 2.104 and g_{xx} = 1.938 can be assigned to O_2^- and Ti^{3+} species respectively [57]. But it has a little increase in the signal intensity of g_{yy} at DT2, suggesting that the level of oxygen vacancies is enhanced due to the gradually accumulation of coke. However, the level of oxygen vacancies is sharply decreased at DT5 and DT10, and the characteristic peaks of g_{zz} and g_{xx} are almost disappeared. Since the signal of g_{yy} is associated with the interaction of e^- and oxygen vacancies, the proper level of coke could facilitate the e^- transferring to the sites of oxygen vacancies. But, with the accumulation of coke, more defects will be produced on the surface of TiO_2, and the e^- may be trapped by the defect of coke.

The optical properties of photocatalysts were also closed related to the photocatalytic performance, the UV–vis, fluorescence and time-resolved PL spectra with different degradation time were also carefully checked. As Fig. 8a shows, the sharply enhanced adsorption intensity was observed on used Au/TiO_2@CNTs with different DT, and also found in TiO_2/CNTs photocatalyst system (Fig. S15a). This is possibly because the amorphous coke in composites can easily adsorb the light irradiation and cause the electron transition [60–62]. However, these excited electrons could easily annihilate at the position of defects and been just released as heat or light due to the numerous defects and poor electron-transfer on amorphous coke. The further PL results also confirm the negative effects of coke on separation of photo-generated e^--h^+ pairs over CNTs-based photocatalyst (Figs. 8c and S15c) [63]. This could be mainly because the coke contains unstable hybridized carbons with numerous defects, which will become the recombination center of photo-generated charge carriers. For TiO_2, the enhanced adsorption intensity at range of 400–600 nm showed that coke could improve the electron transfer at the interfaces of TiO_2 (Fig. 8b), and is also confirmed by PL analysis which shows higher PL emission intensity of pristine TiO_2 than those of catalysts at different time (Fig. 8d). That is, the coke displayed positive effect on the charge carrier transfer and separation for TiO_2, which can be attributed to proper conductivity although weaker than CNTs. Different with TiO_2, the peak intensity in the range of 500–750 nm on Au/TiO_2 was sharply decreased after photocatalytic reaction, which may be attributed to masking effect of coke on LSPR to Au NPs (Fig. S15b). However, the Au/TiO_2 DT samples showed enhanced separation of photo-generated e^--h^+ pairs as PL analysis described (Fig. S15d). Hence, it is confirmed that the positive effects of coke on charge carrier transfer even though it shows negative effects on LSPR to Au NPs. In addition, the effect of coke on the charge transfer was also investigated by time-resolved PL using a TCSPC system (Fig. S16). The average lifetimes (τ_A) of fresh and used photocatalysts with different DT were all calculated by multi-exponential fitting (Table S1). For TiO_2 and Au/TiO_2, their used catalysts show lower values of τ_A than those of pristine samples, suggesting that their used catalysts exhibit better charge transfer and separation efficiency. However, for used TiO_2/CNTs and Au/TiO_2@CNTs, the lifespan of were higher than those of pristine ones, suggesting that the coke can greatly depress the separation and transfer of charge carriers. The enhanced lifespan validated the accumulation of coke would cause the separated e^--h^+ pairs to be released again in the form of light or heat rather than participating in the photocatalytic reaction, and these results were all very consistent with those data from UV–vis and steady state PL analysis.

The influence of coke on photocharges transfer and separation efficiencies was further doubly confirmed by photoelectrochemical method. As shown in Fig. S17a, both fresh and used Au/TiO_2@CNTs photocatalysts show very higher photocurrent response, which is mainly attributed to the contribution of CNTs on the excellent electron transfer [7,22,64]. However, the used Au/TiO_2@CNTs showed obvious decrease of photocurrent response as compared with the fresh one, which could be attributed to poor conductivity of coke and its masking effects of coke on LSPR of Au NPs. Meanwhile, the arc radiuses of Nyquist plots were also increased after photocatalytic degradation, indicating the decreased separation and transfer of charge carriers due to more defect sites from coke becoming the recombination center of photo-generated e^--h^+ pairs (Fig. S18a). Furthermore, the negative effects of coke on charge transfer of TiO_2/CNTs were also observed even though their enhanced intensity of photocurrent response (Figs. S17c and S18c). The enhanced photoresponse on used TiO_2/CNTs may be attributed to the built-in free electrons of coke. In contrast, the used TiO_2 presents a higher photocurrent density and smaller arc radius than that of fresh TiO_2 (Figs. S17b and S18b), which means lower resistance to charge transfer on TiO_2 DT samples. Similar to TiO_2, Au/TiO_2 also

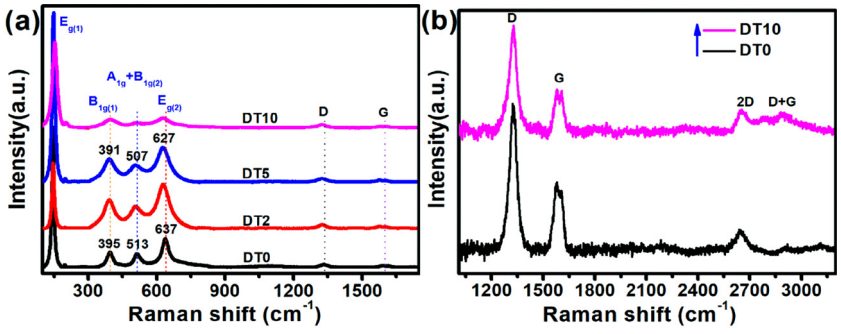

Fig. 7. Raman spectra of Au/TiO_2@CNTs composites with different degradation time.

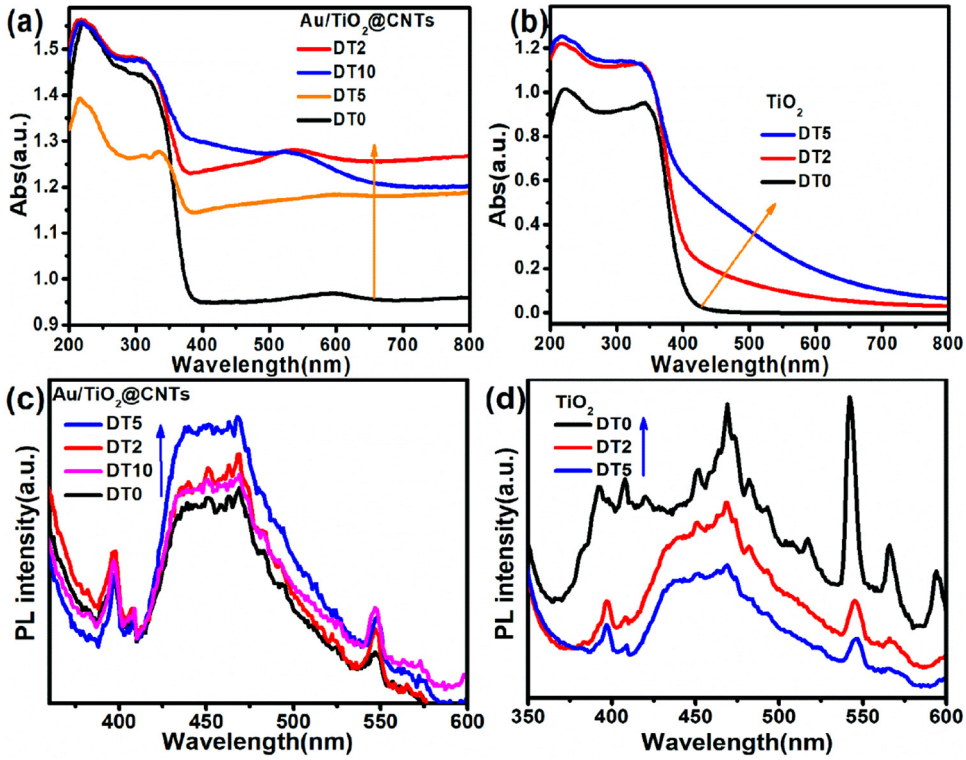

Fig. 8. Optical performance of Au/TiO_2@CNTs and TiO_2 with different degradation time: a and b, UV–vis spectra; c and d, Fluorescence spectra.

shows higher charge transfer efficiency after photocatalytic degradation, but the photocurrent intensity of used 2 h Au/TiO_2 was sharply decreased (Figs. S17d and S18d). This is because the accumulated coke not only produces more defect sites but also causes masking effect on LSPR of Au NPs even it will promote the charge transfer. That is, there is a balance in these photocatalyst systems. When the effects of defect sites and electron transfer associated with coke get a balance, the high recombination of photo-generated e^--h^+ pairs will not happen. These results are very consistent with results of optical properties, and also fully verify the reliability of our coke analysis results for interface charge transfer and separation.

Temperature programmed desorption of oxygen (O_2-TPD) is another crucial method to explore the superficial changes of used catalysts because it can in-site measure the situation of photocatalyst by evaluating the oxygen storage capacity [5,65,66]. As shown in Fig. 9, two main peaks are observed for all samples, which can be assigned to molecularly adsorbed oxygen O_2^- (range from 100 °C to 300 °C) and surface chemically adsorbed oxygen O^- (range from 300 °C to 500 °C) [67]. As for Au/TiO_2@CNTs used, the desorption peaks of O_2^- and O^- are almost unchanged as compared with unused one (Fig. 9a), demonstrating the little influence of coke on O_2^- and O^-. But for TiO_2 (Fig. 9b), a desorption peak with very high intensity of O^- shift from 411 °C to 379 °C, indicating that the coke could enhance the mobility and activation of the chemisorbed oxygen on the TiO_2. However, it is noted that the desorption peaks of O^- on used TiO_2/CNTs and Au/TiO_2 moved to high temperature (Fig. S19), suggesting the negative effects of coke on mobility and activation of the chemisorbed oxygen onto TiO_2/CNTs and Au/TiO_2 [68,69].

To investigate the influence of coke deposited onto catalysts on radicals' changes, the EPR spectra were also conducted using DMPO as the trapping reagent. The four peaks of DMPO − ·OH with intensity of 1:2:2:1 and six characteristic peaks of DMPO − $O_2^{\cdot -}$ are clearly found from the spectra of used Au/TiO_2@CNTs (Fig. 10a and b), and the signal intensities have significant decrease for the degradation catalysts, suggesting less hydroxyl radicals and superoxide radicals was produced after 5 h degradation. Different with used Au/TiO_2@CNTs, the TiO_2 after 5 h degradation shows higher signal intensity of ·OH and $O_2^{\cdot -}$ than that of original TiO_2 (Fig. 10c and d), suggesting that the coke is very beneficial for the separation and transfer of photo-generated charges and the formation of ·OH and $O_2^{\cdot -}$ on TiO_2 to some extent. Based on the optical and photoelectrochemical results, the coke will produce more recombination center and cause masking effects on

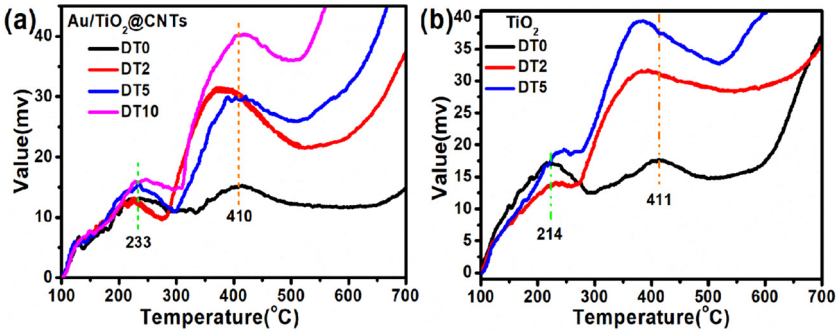

Fig. 9. TPD-O_2 curves of Au/TiO_2@CNTs (a) and TiO_2 (b).

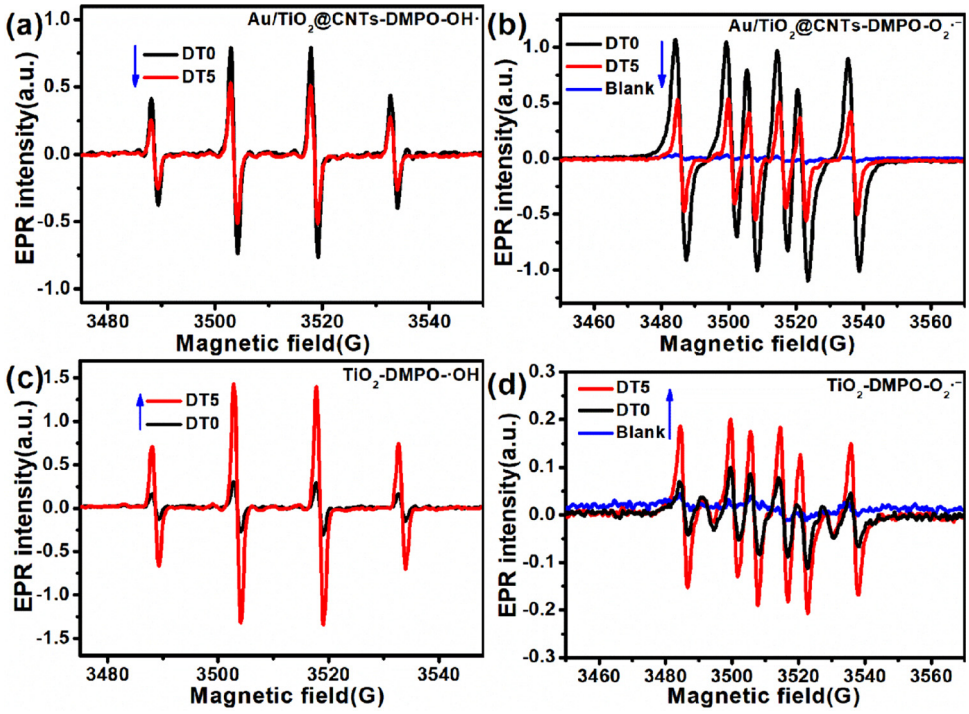

Fig. 10. Radical analysis on Au/TiO_2@CNTs (a, DMPO-˙OH; b, DMPO-O_2˙–) and TiO_2 (c, DMPO-˙OH; d, DMPO-O_2˙–) with different degradation time.

LSPR, and all of which will certainly depress the formation of oxidation radicals on Au/TiO_2@CNTs. But for TiO_2, the coke may act as the media of electron transfer and then substantially enhance the separation efficiency of photo-generated e^--h^+ pairs as well as the formation rate of free radicals. Even so, the used Au/TiO_2@CNTs still remains higher generation efficiencies of oxidation radicals than that of fresh TiO_2 and the used TiO_2. That is the reason why Au/TiO_2@CNTs can maintain long-lasting and stable photocatalytic performance.

According to above results, three possible reasons associated with coke involving the change of superficial state of photocatalysts were presumed: (1) the coke could hinder the absorption and utilization of photons of Au/TiO_2@CNTs used during the photocatalytic degradation; (2) the coke was an instable accumulated impurity carbon with numerous defects, and then increase the recombination of photo-generated e^--h^+ pairs; (3) the competitive degradation and mineralization of coke with degraded VOCs would obviously weakened and then deposited onto catalysts more and more after long time photocatalytic degradation. That is, the photocatalytic performance of Au/TiO_2@CNTs used will be finally decreased and deactivated with the intermediate's growth and accumulated coke to some extent.

Thus, combining the results of intermediates identification with superficial state change of used photocatalysts, the deep deactivation mechanism of used photocatalyst are summarized in Fig. 11,

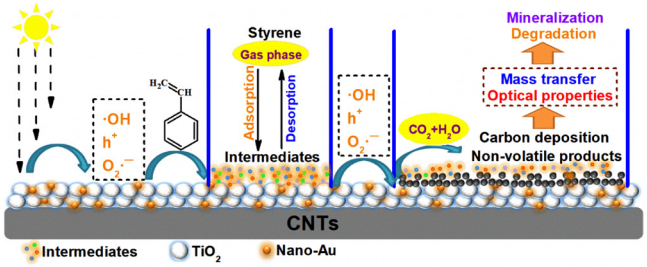

Fig. 11. Schematic diagram of superficial state change on Au/TiO_2@CNTs composites.

respectively. It is because the formation of coke is inseparable from the accumulated intermediates, but what kind of the intermediates and how they are produced and accumulated on photocatalyst and then to form the coke were also explained as followed. Before starting the photocatalytic reaction, the gaseous styrene was firstly adsorbed onto the surface of photocatalysts. That is, large amount of CO_2 and oxidation intermediates are produced due to the styrene fully contacting with the photocatalysts. Meanwhile, large amounts of adsorbed styrene are reacted with numerous free radicals during this process. The photocatalytic transformation mechanism of styrene was tentatively proposed step by step during the reaction course of styrene with ˙OH, to form 2-phenylethyl alcohol and then rapidly transforms into benzoic acid with high boiling points through many steps dehydration reaction, which is consistent with our previous results [44]. With further increase the degradation time, more and more complex intermediates were produced and cannot instantly degraded with limitedly produced free radicals, and lead to the adsorbed intermediates encountering incomplete oxidation reaction and coke formation with complex dehydrogenation reactions. Then the accumulation of intermediates could gradually hinder the mass transfer of gaseous styrene onto the surface of photocatalysts due to the adsorbed sites being occupied. Furthermore, the adsorbed intermediates would substantially consume the free radicals generated on the photocatalyst, which consequently compete with the photocatalytic degradation of styrene. Further, the coke generated from the incomplete oxidation of intermediates not only weakened the light absorption, but hindered the transfer of charge carriers and the formation trend of free radicals. The negative effects of coke would feedback to the surface of photocatalysts, resulting in oxidation ability decreased of photocatalysts, which will speed the formation and accumulation of intermediates on the inversely. The combined negative effects of accumulated intermediates and coke would ultimately make the photocatalysts inactivated. Hence, to ensure the high stability and efficiency of photocatalyst, the enrichment of reactant on the surface of photocatalysts should be avoided, aiming to reduce the accumulation of instantaneous intermediates. Simultaneously, increasing oxygen fluxes ensures the numerous oxidation radicals generated during photocatalytic process to depress the generation of coke. Also, it is necessary

to design photocatalysts with high activity and specific surface area, which is beneficial for the adsorption, mass transfer and advanced oxidation of VOCs and their intermediates.

4. Conclusions

This work showcases the essential reasons why photocatalyst deactivation from the change features of superficial state of used photocatalysts. Although the addition of Au NPs and CNTs could greatly improve the photocatalytic performance of TiO_2, the composite photocatalysts suffered a gradual deactivation process with increasing the photocatalytic reaction time. The thermostability and composition characterizations demonstrated the obvious weight loss and increase of C1 s validated the coke formation during intermediates accumulation on the surface of photocatalysts. Due to its conductivity of carbon chains, the coke could enhance the transfer and separation of charge carriers on TiO_2 and Au/TiO_2, but it has negative effects on TiO_2/CNTs and Au/TiO_2@CNTs due to its numerous defects. Furthermore, the correlation of photocatalytic performance and intermediates accumulation showed that the Au/TiO_2@CNTs system possessed the lowest the accumulation efficiency of intermediates and guaranteed the highest photocatalytic performance. The intermediate accumulation onto photocatalysts was one of the most important affecting factors to form coke and then deactivating photocatalysts. The intermediates accumulation would increase the production of coke and feedback to the surface of photocatalysts, and finally cause the deactivation of photocatalysts during the degradation processes.

CRediT authorship contribution statement

Weiping Zhang: Methodology, Formal analysis, Writing - original draft, Investigation. **Guiying Li:** Writing - review & editing. **Hongli Liu:** Data curation. **Jiangyao Chen:** Formal analysis. **Shengtao Ma:** Methodology, Software. **Meicheng Wen:** Visualization. **Jiejing Kong:** Validation. **Taicheng An:** Supervision, Conceptualization, Writing - review & editing.

Declaration of Competing Interest

The authors declare that they have no known competing financial interests or personal relationships that could have appeared to influence the work reported in this paper.

Acknowledgments

This work was supported by National Natural Science Foundation of China (41731279, 41425015 and 41373102), Guangdong Provincial Key R&D Program (2019B110206002), Local Innovative and Research Teams Project of Guangdong Pearl River Talents Program (2017BT01Z032), Innovation Team Project of Guangdong Provincial Department of Education (2017KCXTD012), China Postdoctoral Science Foundation (2017M622639 and 2018T110851).

Appendix A. Supplementary data

Supplementary material related to this article can be found, in the online version, at doi:https://doi.org/10.1016/j.apcatb.2020.118969.

References

[1] J.Y. Chen, Y. Huang, G.Y. Li, T.C. An, Y.K. Hu, Y.L. Li, J. Hazard. Mater. 302 (2016) 395–403.
[2] N.B. Goodman, A. Steinemann, A.J. Wheeler, P.J. Paevere, M. Cheng, S.K. Brown, Build. Environ. 122 (2017) 116–125.
[3] J.J. Kong, G.Y. Li, M.C. Wen, J.Y. Chen, H.L. Liu, T.C. An, J. Catal. 370 (2019) 88–96.
[4] M.C. Wen, G.Y. Li, H.L. Liu, J.Y. Chen, T.C. An, H. Yamashita, Environ. Sci. Nano 6 (2019) 1006–1025.
[5] Y.B. Li, C.B. Zhang, H. He, J.H. Zhang, M. Chen, Catal. Sci. Technol. 6 (2016) 2289–2295.
[6] Q.N. Song, M. Li, L.L. Wang, X.J. Ma, F. Liu, X. Liu, J. Hazard. Mater. 363 (2019) 119–126.
[7] J.Y. Chen, G.Y. Li, Y. Huang, H.M. Zhang, H.J. Zhao, T.C. An, Appl. Catal. B: Environ. 123–124 (2012) 69–77.
[8] H.L. Liu, Y.P. Ma, J.Y. Chen, M.C. Wen, G.Y. Li, T.C. An, Appl. Catal. B: Environ. 250 (2019) 337–346.
[9] T.C. An, L. Sun, G.Y. Li, Y.P. Gao, G.G. Ying, Appl. Catal. B: Environ. 102 (2011) 140–146.
[10] J. Li, S. Cai, E. Yu, B. Weng, X. Chen, J. Chen, H. Jia, Y. Xu, Appl. Catal. B: Environ. 233 (2018) 260–271.
[11] M.J. Muñoz-Batista, G.R. Bertolini, C.I. Cabello, R. Luque, E. Rodríguez-Castellón, A. Kubacka, M. Fernández-García, Appl. Catal. B: Environ. 238 (2018) 381–392.
[12] Y. Hou, X.Y. Li, Q.D. Zhao, G.H. Chen, C. Raston, Environ. Sci. Technol. 46 (2012) 4042–4050.
[13] A. Truppi, F. Petronella, T. Placido, M. Striccoli, A. Agostiano, M. Curri, R. Comparelli, Catalysts 7 (2017) 100.
[14] S.F. Fu, Y. Zheng, X.B. Zhou, Z.M. Ni, S.J. Xia, J. Hazard. Mater. 363 (2019) 41–54.
[15] X.B. Zhu, C. Jin, X.S. Li, J.L. Liu, Z.G. Sun, C. Shi, X.G. Li, A.M. Zhu, ACS Catal. 7 (2017) 6514–6524.
[16] X. Deng, J. Liu, X. Li, B. Zhu, X.B. Zhu, A. Zhu, Catal. Today 281 (2017) 630–635.
[17] W.P. Zhang, G.Y. Li, H.L. Liu, J.Y. Chen, S.T. Ma, T.C. An, Environ. Sci.-Nano 6 (2019) 948–958.
[18] K. Demeestere, J. Dewulf, H. Van Langenhove, Cri. Rev. Environ. Sci. Technol. 37 (2007) 489–538.
[19] M. Hosseini, S. Siffert, H.L. Tidahy, R. Cousin, J.F. Lamonier, A. Aboukais, A. Vantomme, M. Roussel, B.L. Su, Catal. Today 122 (2007) 391–396.
[20] J.J. Kong, Z.W. Xiang, G.Y. Li, T.C. An, Appl. Catal. B: Environ. 269 (2020) 118755.
[21] J.Z. Li, Y. Ma, Z.F. Ye, M.J. Zhou, H.Q. Wang, C.C. Ma, D.D. Wang, P.W. Huo, Y.S. Yan, Appl. Catal. B: Environ. 204 (2017) 224–238.
[22] T.C. An, J.Y. Chen, X. Nie, G.Y. Li, H.M. Zhang, X.L. Liu, H.J. Zhao, ACS Appl. Mater. Inter. 4 (2012) 5988–5996.
[23] Y.J. Xu, Y.B. Zhuang, X.Z. Fu, J. Phys. Chem. C 114 (2010) 2669–2676.
[24] Z. Tang, F. Li, Y.H. Zhang, X.Z. Fu, Y. Xu, J. Phys. Chem. C 115 (2011) 7880–7886.
[25] J.Y. Shi, J.Y. Chen, G.Y. Li, T.C. An, H. Yamashita, Catal. Today 281 (2017) 621–629.
[26] Y.X. Zhang, B. Gao, G. Li Puma, A. Ray, H.C. Zeng, Sci. Adv. Mater. 2 (2010) 503–513.
[27] J. Li, S.B. Tang, L. Lu, H.C. Zeng, J. Am. Chem. Soc. 129 (2007) 9401–9409.
[28] R.M. Mohamed, I.A. Mkhalid, J. Ind. Eng. Chem. 22 (2015) 390–395.
[29] X. Feng, X.Z. Duan, G. Qian, X.G. Zhou, D. Chen, W.K. Yuan, Appl. Catal. B: Environ. 150-151 (2014) 396–401.
[30] L. Sun, G. Li, S. Wan, T. An, Chemosphere 78 (2010) 313–318.
[31] R.Y. Zhong, Z.S. Zhang, H.Q. Yi, L. Zeng, C. Tang, L.M. Huang, M. Gu, Appl. Catal. B: Environ. 237 (2018) 1130–1138.
[32] Q.H. Chen, Y.J. Xin, X.W. Zhu, Electrochim. Acta 186 (2015) 34–42.
[33] M. Alsawat, T. Altalhi, K. Gulati, A. Santos, D. Losic, ACS Appl. Mater. Inter. 7 (2015) 28361–28368.
[34] Y. Wang, J.G. Yu, W. Xiao, Q. Li, J. Mater. Chem. A 2 (2014) 3847–3855.
[35] C.K. Ngaw, Q.C. Xu, T.T.Y. Tan, P. Hu, S.W. Cao, J.S.C. Loo, Chem. Eng. J. 257 (2014) 112–121.
[36] S.G. Wang, Z.R. Du, C.X. Kong, P.F. Li, J.L. Xu, C.X. Wang, J.H. Wang, Nano 9 (2014) 1450003.
[37] Q.Q. Ding, Y.X. Zhang, G.Z. Wang, H.J. Zhou, H.M. Zhang, RSC Adv. 6 (2016) 18958–18964.
[38] H.J. Chen, L. Shao, Q. Li, J.F. Wang, Chem. Soc. Rev. 42 (2013) 2679–2724.
[39] S. Kim, I. Ali, J. Kim, J. Ind. Eng. Chem. 66 (2018) 370–380.
[40] F. Xu, J.F. Chen, S. Kalytchuk, L. Chu, Y.R. Shao, D.X. Kong, K.H. Chu, P.L. Sit, W.Y. Teoh, J. Catal. 354 (2017) 1–12.
[41] L. Xu, L. Yang, E. Johansson, Y.H. Wang, P.K. Jin, Chem. Eng. J. 350 (2018) 1043–1055.
[42] D.W. Ding, K. Liu, S.N. He, C.B. Gao, Y.D. Yin, Nano Lett. 14 (2014) 6731–6736.
[43] Z. Lu, M. Piernavieja-Hermida, C.H. Turner, Z.L. Wu, Y. Lei, J. Phys. Chem. C 122 (2018) 1688–1698.
[44] J.Y. Chen, Z.G. He, Y.M. Ji, G.Y. Li, T.C. An, W.Y. Choi, Appl. Catal. B: Environ. 257 (2019) 117912.
[45] Q.L. Liu, J.M. Li, Z. Zhao, M.L. Gao, L. Kong, J. Liu, Y.C. Wei, J. Catal. 344 (2016) 38–52.
[46] S. Weon, W. Choi, Environ. Sci. Technol. 50 (2016) 2556–2563.
[47] R. Fiorenza, M. Bellardita, L. D'Urso, G. Compagnini, L. Palmisano, S. Scirè, Catalysts 6 (2016) 121.
[48] W.Q. Cui, J. He, H. Wang, J.S. Hu, L. Liu, Y.H. Liang, Appl. Catal. B: Environ. 232 (2018) 232–245.
[49] Z.J. Yu, X. Hu, P. Jia, Z.M. Zhang, D.H. Dong, G.Z. Hu, S. Hu, Y. Wang, J. Xiang, Appl. Catal. B: Environ. 237 (2018) 538–553.
[50] H. Wang, L. Sun, Z. Sui, Y. Zhu, G. Ye, D. Chen, X. Zhou, W. Yuan, Ind. Eng. Chem. Res. 57 (2018) 8647–8654.
[51] M. Mokhtar Mohamed, G. Osman, K.S. Khairou, J. Environ. Chem. Eng. 3 (2015) 1847–1859.
[52] A. Matilainen, E. Gjessing, T. Lahtinen, L. Hed, A. Bhatnagar, M. Sillanpaa, Chemosphere 83 (2011) 1431–1442.
[53] J. Li, H.C. Zeng, Chem. Mater. 18 (2006) 4270–4277.
[54] D. Zhan, Z.H. Ni, W. Chen, L. Sun, Z.Q. Luo, L.F. Lai, T. Yu, A.T.S. Wee, Z.X. Shen, Carbon 49 (2011) 1362–1366.

[55] S. Lee, G. Baek, J.-H. Lee, D.W. Choi, B. Shong, J.S. Park, Appl. Surface Sci. 458 (2018) 864–871.
[56] H.P. Yang, Y.C. Zhang, X.F. Fu, S.S. Song, J.M. Wu, Acta Phys.-Chim. Sin. 29 (2013) 1327–1335.
[57] J. Priebe, J. Radnik, A. Lennox, M. Pohl, M. Karnahl, D. Hollmann, K. Grabow, U. Bentrup, H. Junge, M. Beller, A. Brückner, ACS Catal. 5 (2015) 2137–2148.
[58] E.I. Seck, J.M. Doña-Rodríguez, C. Fernández-Rodríguez, O.M. González-Díaz, J. Araña, J. Pérez-Peña, Appl. Catal. B: Environ. 125 (2012) 28–34.
[59] X.M. Yu, B. Kim, Y.K. Kim, ACS Catal. 3 (2013) 2479–2486.
[60] S. Komatsuda, Y. Asakura, J. Vequizo, A. Yamakata, S. Yin, Appl. Catal. B: Environ. 238 (2018) 358–364.
[61] L. Xu, X. Bai, L.K. Guo, S.J. Yang, P.K. Jin, L. Yang, Chem. Eng. J. 357 (2019) 473–486.
[62] N. An, Y.W. Ma, J.M. Liu, H.Y. Ma, J.C. Yang, Q.C. Zhang, Chin. J. Catal. 39 (2018) 1890–1900.
[63] J.Q. Yang, X.J. Li, C.M. Liu, G.L. Ma, F. Gao, Chin. Phys. B 24 (2015) 116103.
[64] X.J. She, J.J. Wu, H. Xu, Z. Mo, J.B. Lian, Y.H. Song, L. Liu, D.L. Du, H.M. Li, Appl. Catal. B: Environ. 202 (2017) 112–117.
[65] N. Comsup, J. Panpranot, P. Praserthdam, J. Ind. Eng. Chem. 16 (2010) 703–707.
[66] Y.N. Chen, D.S. Liu, L.J. Yang, M. Meng, J. Zhang, L.R. Zheng, S.Q. Chu, T.D. Hu, Chem. Eng. J. 234 (2013) 88–98.
[67] C.S. Deng, B. Li, L.H. Dong, F.Y. Zhang, M.G. Fan, G.Z. Jin, J.B. Gao, L.W. Gao, F. Zhang, X.P. Zhou, Phys. Chem. Chem. Phys. 17 (2015) 16092–16109.
[68] S. Bhardwaj, A. Pal, K. Chatterjee, T. Rana, G. Bhattacharya, S. Sinha Roy, P. Chowdhury, G. Sharma, S. Biswas, J. Mater. Sci-Mater. Electron. 29 (2018) 18209–18220.
[69] L. Shi, Z. Li, T.D. Dao, T. Nagao, Y. Yang, J. Mater. Chem. A 6 (2018) 12978–12984.